Frontiers in Bioscience Landmark

Front. Biosci. (Landmark Ed) **2025**; 30(6): 38957
https://doi.org/10.31083/FBL38957

Original Research

Multi-omics Analysis Reveals Molecular Subtype of Mitochondrial Oxidative Stress and Prognostic Model Development in Sepsis

Baolong Zhu[1], Jinxiang Wang[2], Yan Wang[1,*]

[1]Department of Infectious Diseases, Qilu Hospital (Qingdao), Cheeloo College of Medicine, Shandong University, 266000 Qingdao, Shandong, China
[2]Department of Respiratory and Critical Care Medicine, Qilu Hospital (Qingdao), Cheeloo College Medicine, Shandong University, 266000 Qingdao, Shandong, China
*Correspondence: 18561811929@163.com (Yan Wang)

Academic Editors: Ming-Wei Lin and Francesco Gavelli
Submitted: 11 March 2025 Revised: 2 May 2025 Accepted: 27 May 2025 Published: 20 June 2025

Abstract

Background: Sepsis is a prevalent disease with high mortality involving severe systemic inflammatory responses. Although the mechanisms underlying sepsis have been widely explored, the occurrence and exacerbation of sepsis remain unclear, with limited therapeutic options. Inflammation and mitochondrial oxidative stress have been proposed as primary factors in the development of sepsis. **Methods**: In the present research, normal and sepsis samples were obtained from the Gene Expression Omnibus (GEO) database (GSE54514, GSE65682, and GSE95233). To identify the key mitochondrial oxidative stress-related gene (MOSRG) signature associated with sepsis, both weighted gene co-expression network analysis (WGCNA) and differential expression analysis were conducted. Least Absolute Shrinkage and Selection Operator (LASSO) analysis and univariate and multivariate Cox analysis were used to construct the prognostic risk model for sepsis. Immune infiltration characteristics were analyzed using the Estimation of STromal and Immune cells in MAlignant Tumor tissues using Expression data (ESTIMATE) and single-sample Gene Set Enrichment Analysis (ssGSEA) algorithms. Single-cell RNA sequencing and *in vitro* experiments provided additional evidence for the pivotal role of RNA-binding protein, ribonuclease 2 (*RNASE2*) in the regulation of mitochondrial oxidative stress in sepsis. **Results**: Three MOSRGs *RNASE2*, CX3C chemokine receptor 1 (*CX3CR1*), and epoxide hydrolase 2 (*EPHX2*) were recognized as potential diagnostic indicators for sepsis in this study. The immune infiltration analysis provides strong evidence that three biomarkers were linked to immune-related mechanisms involved in the pathogenesis of sepsis. The pivotal role of RNASE2 in regulating mitochondrial oxidative stress during sepsis was confirmed using single-cell RNA-seq analysis and validated by *in vitro* molecular biology experiments. Inhibition of *RNASE2* was found to significantly mitigate mitochondrial oxidative stress injury in sepsis. **Conclusion**: This research underscores the significant impact of mitochondrial oxidative stress-related genes on immune regulation in sepsis and highlights the potential therapeutic implications of candidate biomarkers.

Keywords: sepsis; mitochondrial oxidative stress; immune infiltration; RNASE2; prognostic risk model

1. Introduction

Sepsis is a lethal organ dysfunction syndrome that is accompanied by a systemic inflammation caused by a dysregulated host immune response [1]. It affects millions of people worldwide with high mortality and increasing incidence, representing the major cause of death in critically ill patients [2]. Sustained excessive inflammation and dysfunction across multiple organs are key contributors to the morbidity and mortality associated with sepsis. Early recognition and fluid resuscitation, empiric intravenous antibiotic therapy, source control of infection, achieving hemodynamic stability are the key cornerstones of early management in sepsis [3,4]. Notably, these therapeutic interventions are not incredibly effective in countering the persistent dysregulation of the host immune response and the subsequent prolonged immunosuppression. There is still no broadly applicable effective clinical treatment for sepsis, and the chronic risk of mortality after sepsis in patients remains unacceptably high [5]. Thus, an improved understanding of the underlying mechanisms in sepsis is warranted to develop new therapeutic strategies for treatment.

Mitochondria are increasingly implicated as a critical factor in sepsis pathogenesis. Numerous investigations have provided insights into the mitochondrial dysfunction is tightly associated with sepsis-induced organ dysfunction [6,7]. Mitochondria are the crucial membrane-bound organelles involved in cellular metabolism, reactive oxygen species (ROS) generation, energy generation and Ca^{2+} homeostasis. The excessive ROS generation by mitochondria is suggested to be a pivotal issue of the high metabolic burden during sepsis, which progressed into organ dysfunction [8]. The clinical evidence has been well established that a state of severe oxidative stress is encountered in sepsis patients, marked by elevated concentrations of free radicals and lipid peroxidation products, along with a reduction in antioxidant defenses [9]. It has been stated that mitochondria oxidative stress was the hub of innate immune signals and inflammation during sepsis [10]. Previous studies documented that mitochondrial dysfunction mediated a

vicious hyperinflammation cycle through catalyzing generation of ROS, insufficient energy production, and cellular metabolic disorders to promote oxidative damage in sepsis [11,12]. Literature showed that ROS generation by mitochondria could modulate inflammatory responses by activating multiple signal transduction cascades, which is essential for regulating immune responses against pathogens [13]. It was assumed that mitochondrial oxidative stress may modulate inflammation responses in the development of sepsis. Thus, understanding the role of mitochondrial oxidative stress and immune in the pathophysiologic mechanism of sepsis is paramount to the detection, treatment and prognosis of sepsis.

Comprehensive bioinformatics methods provide an opportunity to identify effective biomarkers for disease diagnosis, prognosis, prevention, and to better unravel the underlying molecular mechanisms of sepsis [14]. Hence, there is a compelling need to investigate the role of mitochondrial oxidative stress-related gene (MOSRG) involved in sepsis, greatly facilitating therapeutic decisions for sepsis diagnosis, treatment and prognostic prospects. In the current study, we successfully identified 59 differentially expressed MOSRG (DE-MOSRG) between normal and sepsis samples using public databases. Additionally, a prognostic risk model was constructed to indicate the clinical traits and prognostic outcomes in sepsis based on DE-MOSRG. Immune infiltration characteristics analyses and single-cell sequencing results further indicated a possible connection between the DE-MOSRG signature and immune infiltration in sepsis. This study aims to explore the accurate and faithful candidate biomarkers for sepsis early diagnosis and treatment.

2. Materials and Methods

2.1 Preprocessing of Transcriptome Matrix

Based on the Gene Expression Omnibus (GEO) database (https://www.ncbi.nlm.nih.gov/), three transcriptomic datasets (GSE54514, GSE65682, and GSE95233) including normal control (NC) and sepsis (SP) samples were retrieved and downloaded. Gene annotation was performed using the corresponding platform annotation files with Perl scripts. To correct for batch effects and normalize expression data across datasets, the "sva" package was employed within the R environment. Following the exclusion of sepsis samples lacking prognostic data, 100 NC samples and 479 SP samples remained for subsequent analyses.

2.2 Weighted Gene Co-Expression Network Analysis

To identify sepsis clinical phenotypes associated with gene modules, the "WGCNA" R package was utilized to build a weighted gene co-expression network. First, we selected the 5000 most significantly ranked genes with the highest variance across all samples from the input gene expression matrix to enhance computational efficiency. Next, we chose a soft-threshold power to ensure the scale-free topology of the network. By following the scale-free topology criterion, an appropriate soft threshold was determined by calculating the network topology fit index (R^2) for different power values, selecting the minimum power where $R^2 > 0.85$. The adjacency matrix was computed based on gene expression correlations and subsequently converted into a Topological Overlap Matrix (TOM) to quantify the similarity between genes. Using the dynamic tree cut method, genes were grouped into modules with a minimum module size of 30. Module eigengenes (MEs) were utilized to assess the correlation between each gene module and phenotypic traits, identifying modules highly correlated with the target phenotype. To further refine candidate genes, candidate genes within key modules were identified according to their gene significance and module membership values, defining candidate genes as those with high gene significance (GS) and module membership (MM).

2.3 Identification of Differentially Expressed Mitochondrial Oxidative Stress-Related Gene Signatures

Using the GeneCard database (https://www.genecards.org/), we identified a series of MOSRG for further exploratory analysis (**Supplementary Table 1**). A differential expression threshold was set at $|\text{fold change}| \geq 2$ and $p.\text{adjust} < 0.05$. With the "limma" and "heatmap" R script, differential gene expressions between the NC group and SP group were analyzed and visualized. By applying the "venn" R script, we performed an analysis of genes exhibiting differential expressions, key gene modules, and MOSRG signatures, identifying the intersecting genes as key differentially expressed MOSRG signatures. To explore potential molecular regulatory mechanisms, we used the "clusterProfiler" R script to conduct Gene Ontology (GO) and Kyoto Encyclopedia of Genes and Genomes (KEGG) enrichment analyses on the differentially expressed MOSRG.

In addition, using the STRING database, we predicted protein-protein interactions (PPI) between different genes (https://string-db.org/).

2.4 MOSRG Prognostic Scoring Model Development and Validation in Sepsis

With the "survival" R package univariate Cox regression analysis was made, based on the expression patterns of the MOSRG signature and the clinical prognosis data of sepsis samples to identify MOSRG signatures associated with sepsis prognosis. A Least Absolute Shrinkage and Selection Operator (LASSO) function model was constructed using the "glmnet" R script to determine prognostic MOSRG signature variables, followed by multivariate Cox analysis to calculate the risk coefficients for each signature variable. Based on the prognostic variable risk coefficients and expression levels, we built the MOSRG score for each SP and developed the MOSRG scoring model. The MOSRG score formula is as follows: MOSRG score =

CX3C chemokine receptor 1 (*CX3CR1*) × –2.056 + epoxide hydrolase 2 (*EPHX2*) × –1.720 + RNA-binding protein, ribonuclease 2 (*RNASE2*) × 2.065. By the optimal cutoff value for the 28-day clinical prognosis outcomes, we classified the samples into low- and high-MOSRG score subgroups and plotted a scatter plot of the subgroup classifications using the "ggplot2" R script. The "survival" and "survivalROC" R scripts were employed to generate 28-day clinical survival curves, as well as time-dependent receiver operating characteristic (ROC) curves for 7-day, 14-day, and 28-day outcomes. Using the "caret" machine learning algorithm, sepsis samples were split into two independent cohorts, using a 7:3 ratio for the training and validation groups. Using the risk coefficients and expression profiles from the MOSRG prognostic signature, we computed MOSRG scores for both cohorts. Prognosis and time-dependent ROC curves were then generated for both cohorts.

2.5 Independent Prognostic Value Assessment the Nomogram Diagnostic Model Construction

Using clinical baseline data of SP and the MOSRG scoring signature, we performed both multivariate and univariate Cox analyses by "survminer" R script to assess the independent prognostic significance in predicting the clinical outcomes. By conducting "rms" R script, we constructed a diagnostic nomogram incorporating clinicalpathological characteristics and the MOSRG score to estimate survival probabilities of the samples. Calibration curves and the concordance index (C-index) were created using the "regplot" and "pec" R scripts to assess the reliability of the nomogram diagnostic model and the accuracy of each variable. Using the "ggDCA" R script, we plotted the decision curve analysis (DCA) for different clinicalpathological characteristics, the nomogram model, and the MOSRG score.

2.6 Identification of MOSRG Molecular Subtypes and Assessment of Immune Microenvironment Composition

Using the "ConsensusClusterPlus" R script, we classified the sepsis samples based on the "K-means" algorithm with a classification range of k = 2 to 9. The optimal classification was determined based on the delta area curve and consensus cumulative distribution function (CDF) curve results. Clinical survival curves for the 28-day outcomes of the molecular subgroups of SP were plotted using the "survival" R script. We assessed the immune score and Estimation of STromal and Immune cells in MAlignant Tumor tissues using Expression data (ESTIMATE) score using the "estimate" R package. To quantify immune infiltration status, single-sample Gene Set Enrichment Analysis (ssGSEA) analysis was conducted using the "Gene Set Variation Analysis (GSVA)" R package, with marker genes for 23 immune cell types. Additionally, using the reference gene list for KEGG signaling pathways, we utilized the "GSVA" R script to calculate the differential regulated signaling pathways.

2.7 Single-Cell Sequencing Data Acquisition and Preprocessing

The single-cell RNA sequencing (scRNA-seq) dataset GSE167363, comprising data from sepsis patients, was retrieved from the GEO database for this study [15] (https://www.ncbi.nlm.nih.gov/). Following the exclusion of samples that did not meet inclusion criteria, peripheral blood mononuclear cells (PBMCs) from 2 healthy controls (HCs) and 5 SPs were selected for downstream analysis. First, the raw data underwent quality control processing using the "Seurat" package in R (v4.0.5, Satija Lab, New York, NY, USA), filtering cells with gene counts between 200 and 5000 and mitochondrial gene content below 10%, while removing low-expressed genes. The dataset was normalized via the "LogNormalize" method, followed by selection of the 2000 most variable genes. To control for batch effects across different experimental conditions, we applied the FindIntegrationAnchors and IntegrateData functions to integrate the samples. After data normalization, principal component analysis (PCA) was performed to reduce data dimensionality, selecting the top 20 principal components for cell clustering. A K-nearest neighbor (KNN) graph was constructed using the FindNeighbors and FindClusters functions for clustering, and cell population distribution was visualized using t-distributed Stochastic Neighbor Embedding (t-SNE) and Uniform Manifold Approximation and Projection (UMAP) algorithms. Cell types were annotated using the SingleR algorithm and known marker genes, leading to the cell subpopulation identification such as Natural Killer (NK) cells, platelets, monocytes, and neutrophils. Finally, we further analyzed and displayed their expression distribution of prognostic-related genes using VlnPlot and FeaturePlot.

2.8 Cell Culture

The cell line RAW264.7 was validated through short tandem repeat (STR) profiling and confirmed to be free of mycoplasma contamination. RAW264.7 murine macrophages (obtained from the Shanghai Cell Bank, Chinese Academy of Sciences, Shanghai, China) were cultured in Dulbecco's Modified Eagle Medium (DMEM; Cat# C11995500BT, Beyotime Biotechnology, Shanghai, China) supplemented with 10% heat-inactivated fetal bovine serum (FBS, Cat# 164210-50, Tianhang Bio, Shaoxing, China), 100 U/mL penicillin and 100 µg/mL streptomycin (Cat# C0222, Beyotime Biotechnology, Shanghai, China). Cells were incubated at 37 °C in a humidified atmosphere containing 5% CO_2, and the medium was refreshed every 2–3 days to maintain optimal growth conditions.

2.9 siRNA Transfection

RAW264.7 cells were cultured in DMEM and seeded in 6-well plates at a density of 2×10^5 cells per well until reaching approximately 50–60% confluency. siRNA or negative control siRNA (siNC) was diluted in serum-free Opti-MEM medium (Cat# 31985-070, Gibco, New York, USA) to a final concentration of 50 nM and mixed with Lipofectamine 3000 transfection reagent (Cat# L3000-015, Invitrogen, Carlsbad, USA) according to its instructions. The transfection mixture was gently added to each well and incubated for 48 hours. Subsequently, the siRNA-transfected cells were stimulated with 500 ng/mL lipopolysaccharide (LPS, Cat# L2630, Sigma-Aldrich, St. Louis, USA) for an additional 12 hours. The target sequence was as follow: RNASE2 siRNA, 5′-AGAACAUGUAAGGGCUUAAAUTT-3′. siRNA for RNASE2 was generated by Sangon Biotech (Shanghai, China).

2.10 Detection of ROS Using DCFH-DA Staining

Cells were seeded in 6-well plates at a density of 1×10^5 cells per well and incubated overnight to allow for adherence. Subsequently, the culture medium was discarded, and each well was incubated with 1 mL of serum-free medium containing 10 µM 2′,7′-dichlorodihydrofluorescein diacetate (DCFH-DA; Cat# S0033S, Beyotime, Shanghai, China) to allow for intracellular ROS detection. Cells were incubated in the dark for half an hour. Following incubation, cells were washed three times with PBS, each for 5 minutes, to remove unreacted probes. Fluorescence microscopy (Olympus IX73, Tokyo, Japan) was used for detection with an excitation and emission wavelength of 488 nm and 525 nm.

2.11 Detection of Mitochondrial Membrane Potential Using JC-1 Staining

Cells were plated in a 6-well plate at a density of 1×10^5 cells per well and incubated overnight until adherent. The medium was then discarded, and 1 mL serum-free medium containing 5 µg/mL JC-1 (5,5′,6,6′-Tetrachloro-1,1′,3,3′-tetraethylbenzimidazolylcarbocyanine iodide, Cat# C2006, Beyotime, Shanghai, China) was added, incubating in the dark for 20 minutes. After two washes with pre-cooled PBS, fluorescence microscopy was used for detection. For JC-1 monomers and aggregates, the excitation wavelength and emission wavelength were 485, 525 nm and 530, 590 nm respectively.

2.12 Detection of Malondialdehyde (MDA)

Cells were harvested, homogenized with Radio-Immunoprecipitation Assay (RIPA) lysis buffer, centrifuged to collect the supernatant. Detection was performed following the instructions provided with the MDA kit (Cat# S0131S, Beyotime, Shanghai, China). Main steps included mixing samples with working solution, incubating at 37 °C, centrifuging, and measuring absorbance of the supernatant. Absorbance was quantified at a wavelength of 530 nm, and MDA concentration was determined.

2.13 Detection of Inflammatory Markers Using ELISA Kits

The levels of IL-1β, IL-6, and TNF-α in the culture supernatants were quantified using enzyme-linked immunosorbent assay (ELISA) kits (Beyotime, Shanghai, China). First, the cell supernatant was diluted to an appropriate concentration and added to 96-well plates pre-coated with specific antibodies. Then, standards and samples were added with 1-hour incubation. After thorough washing, a secondary antibody (provided in the ELISA kit) conjugated with an enzyme was added with 30 minutes incubation. Finally, substrate solution was added and the absorbance was measured at 450 nm (BioTek, Winooski, VT, USA) after 30 minutes. The supernatant concentrations were calculated by the standard curve.

2.14 CCK-8 Assay

Cells were seeded at a density of 5000 cells per well in 96-well plates and incubated overnight to allow adherence. 10 µL of Cell Counting Kit-8 (CCK-8) solution (Cat# C0037, Beyotime, Shanghai, China) was added to each well followed by 2 hours incubation. Absorbance of each well was measured at 450 nm. After the blank control absorbance comparison, cell viability was calculated.

2.15 Western Blotting

Cells were harvested and lysed using an appropriate volume of RIPA lysis buffer, and centrifuged to collect the supernatant. Protein samples were resolved using electrophoresis on a 10% sodium dodecyl sulfate - polyacrylamide gel electrophoresis (SDS-PAGE) gel, followed by transfer of the separated proteins to a polyvinylidene fluoride (PVDF) membrane (Cat# IPVH00010, Millipore, Darmstadt, Germany). After 1 hour block with 5% non-fat milk in (Tris-buffered saline containing 0.1% Tween-20 (TBS-T), Cat# P1379, Sigma-Aldrich, St. Louis, MO, USA, pH 7.4), the membrane was incubated with RNASE2 antibody (1:1000, A9949, ABclonal, Wuhan, China) and β-actin antibody (1:2000, ab8226, Abcam, Cambridge, MA, USA) at 4 °C overnight, TBS-T washed three times, and exposed to the appropriate secondary antibody (Rabbit anti-secondary antibody, 1:20,000, ab288151; Mouse anti-secondary antibody, 1:20,000, ab6728, Abcam, Cambridge, USA) at room temperature for one hour. After that, Enhanced chemiluminescence (ECL) substrate (Cat# P0018FS, Beyotime, Shanghai, China) was used for detection, and the imaging system (ChemiDoc, Bio-Rad, Hercules, CA, USA) was used for capturing and analyzing images.

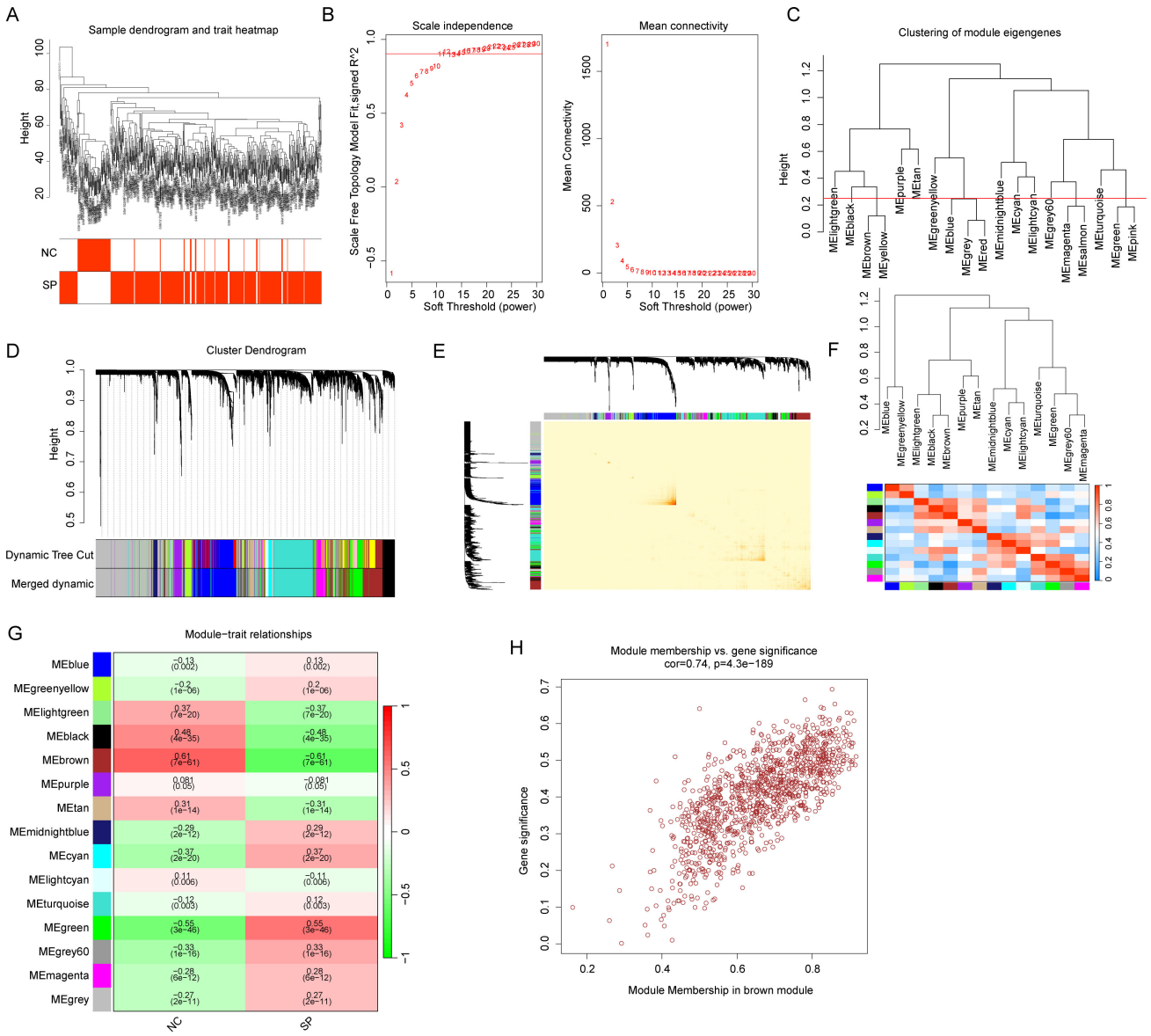

Fig. 1. WGCNA-based identification of key gene modules correlated with clinical traits. (A) Clustering analysis of samples. (B) Determination of the soft-thresholding power (β). (C) Cluster dendrogram analysis of different gene modules. (D) Dynamic tree cutting analysis. (E) Correlation analysis of genes within different gene modules. (F) Correlation analysis of gene modules. (G) Correlation analysis between clinical traits and gene modules. (H) Scatter plot analysis of module membership versus gene significance. WGCNA, weighted gene co-expression network analysis; NC, normal control; SP, sepsis.

2.16 Statistical Analysis

Statistical analyses were conducted using Perl software (v5.30.0; The Perl Foundation, Walnut, CA, USA), R software (v4.3.1; The R Foundation for Statistical Computing, Vienna, Austria), GraphPad Prism (v9.5.0; GraphPad Software, San Diego, CA, USA) and SPSS 17.0 (SPSS Inc., Chicago, IL, USA). All experiments were independently repeated three times to ensure data accuracy and reproducibility. For comparisons between two groups, the unpaired Student's *t*-test was used for normally distributed data, while the Wilcoxon rank-sum test was applied for non-normally distributed data. For comparisons among more than two groups, one-way analysis of variance (ANOVA) followed by Tukey's multiple comparisons test was conducted. The normality test is performed using the "shapiro.test" function in the R language. Correlation analysis was performed using Pearson's correlation coefficient to assess the relationship between MOSRG scores and immune cell infiltration levels. Multiple testing corrections were applied using the Benjamini-Hochberg method, and adjusted p-values < 0.05 were considered statistically significant. Data are presented as mean $\pm$ standard deviation (SD), with significance levels indicated as $^{*}p < 0.05$, $^{**}p < 0.01$, $^{***}p < 0.001$.

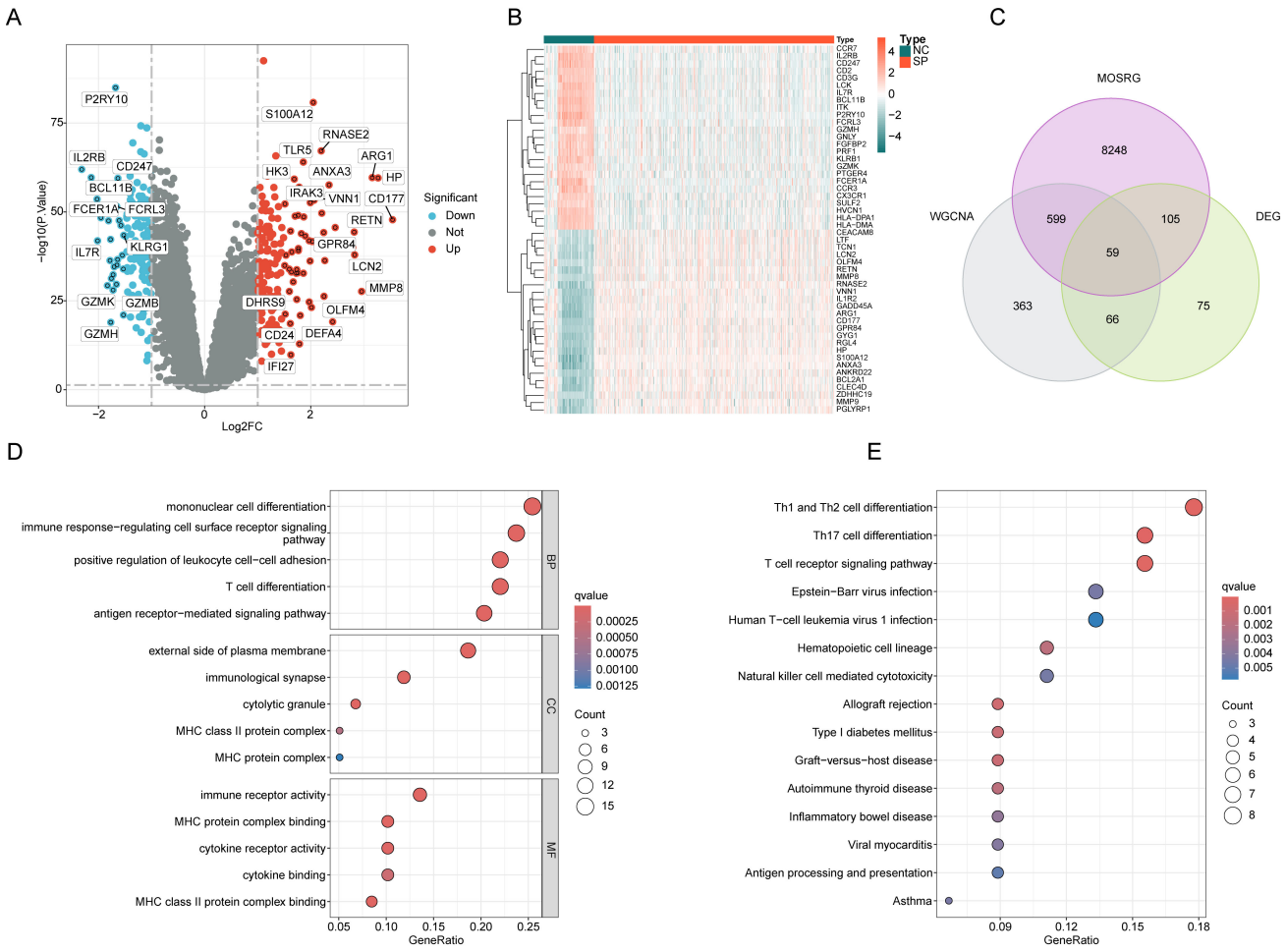

Fig. 2. Screening and enrichment analysis of differentially expressed MOSRG signatures. (A) Differential gene expression analysis between NC and SP groups. Filtering thresholds: |fold change| $\geq$2 and *p*.adjust $<$ 0.05; red: upregulated genes, blue: downregulated genes. (B) Heatmap analysis of differentially expressed gene signatures. (C) Identification of differentially expressed MOSRG signatures. (D,E) KEGG and GO enrichment analysis. MOSRG, mitochondrial oxidative stress-related gene; KEGG, Kyoto Encyclopedia of Genes and Genomes; GO, Gene Ontology; DEG, differentially expressed gene; MHC, major histocompatibility complex; BP, biological process; CC, cellular component; MF, molecular function.

3. Results

3.1 Identification of Key Gene Modules Associated with Sepsis Using WGCNA

To uncover critical gene modules linked to sepsis, we integrated three GEO datasets and extracted data from 100 NC samples and 479 SP samples with 28-day survival prognosis information to construct the WGCNA model. According to the gene expression matrix, we performed clustering analysis using a dendrogram to identify and exclude outlier samples (Fig. 1A). With a soft-thresholding power (β) set at 11, we constructed a scale-free network and identified distinct gene modules from the transcriptomic matrix (Fig. 1B). As shown in Fig. 1C, the clustering tree results displayed the distribution of each gene module (height = 0.25). Similar gene modules were merged by algorithm "dynamic tree cut", resulting in 14 independent gene modules (Fig. 1D). Correlation analysis was employed to evaluate potential associations between genes within each module, revealing that there were no significant correlations between gene matrices within each module (Fig. 1E). Additionally, the correlation results between gene module members demonstrated significant independence among module members (Fig. 1F). Using Pearson's correlation algorithm, we assessed the associations between each gene module and clinical traits. The brown module was significantly positively correlated with NC traits (r = 0.61, $p = 7 \times 10^{-61}$) and exhibited a strong negative correlation with SP traits (r = –0.61, $p = 7 \times 10^{-61}$), suggesting it may be the module most relevant to clinical traits (Fig. 1G). Moreover, scatter plot analysis showed a strong positive correlation between module membership and gene significance within the brown module (r = 0.74, $p = 4.3 \times 10^{-189}$) (Fig. 1H).

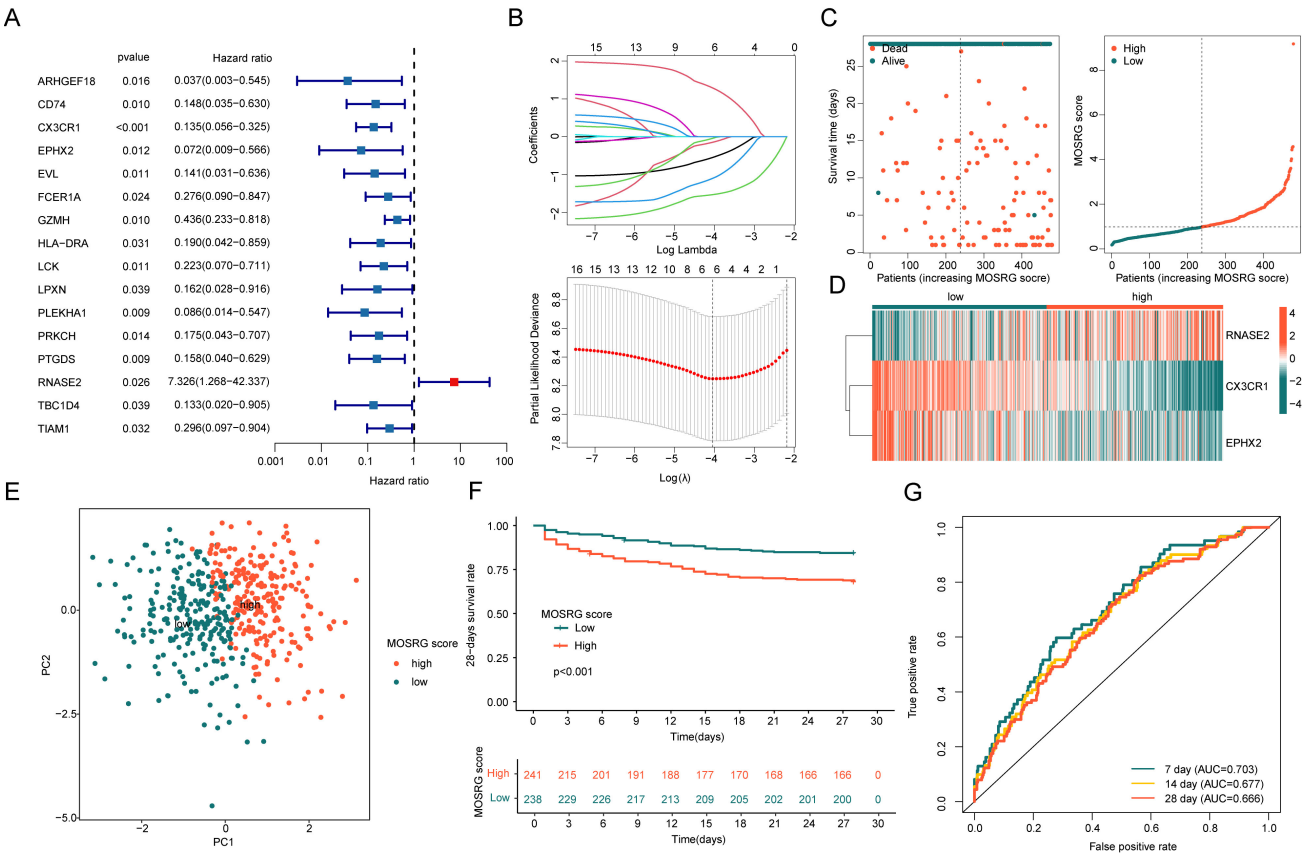

Fig. 3. Construction of a prognostic risk model based on MOSRG signatures in sepsis. (A) Identification of MOSRG signatures associated with SP prognosis using univariate Cox analysis. (B) Construction of the LASSO model to determine MOSRG feature prognostic variables. (C,D) Development of the MOSRG scoring prognostic system. (E) Principal component analysis (PCA) plot analysis. (F) 28-day clinical survival curves analysis for MOSRG scoring subgroups. (G) Time-dependent ROC curve analysis. LASSO, Least Absolute Shrinkage and Selection Operator; ROC, receiver operating characteristic; AUC, area under the curve; RNASE2, RNA-binding protein, ribonuclease 2; CX3CR1, CX3C chemokine receptor 1; EPHX2, epoxide hydrolase 2.

3.2 Identification of Differentially Expressed Key MOSRG Signatures and Enrichment Analysis

Using a differential threshold of $|FC| > 2$ and $p.adjust < 0.05$, we analyzed gene expression patterns between the NC and SP groups, identifying 305 significantly differentially expressed gene signatures (Fig. 2A,B). Venn diagram analysis revealed the intersection of differentially expressed genes, WGCNA and MOSRG signatures, identifying 59 key MOSRG signatures with differential expression (Fig. 2C). Based on enrichment analysis algorithms, we evaluated the potential molecular regulatory mechanisms of the 59 DE-MOSRG in sepsis. GO enrichment analysis indicated that these DE-MOSRG signatures were associated with immune regulatory functions. KEGG enrichment analysis showed that these DE-MOSRG signatures were involved in regulating immune cell receptor signaling pathways (Fig. 2D,E).

3.3 Development of the MOSRG Scoring System for Sepsis

We further assessed the prognostic value of the 59 MOSRG signatures in sepsis and constructed a prognostic risk model to indicate clinical survival outcomes. By integrating the clinical data and MOSRG signature expression features from 479 SP samples, the prognostic value of each variable in SP was assessed by univariate Cox regression analysis. This analysis identified 16 MOSRG signatures associated with SP prognosis, including 15 beneficial factors and one risk factor (Fig. 3A). Further analysis using LASSO regression identified 6 MOSRG features relevant to SP prognosis (Fig. 3B). Subsequently, to determine the independent prognostic impact of these six features, multivariate Cox regression analysis was carried out. The results indicated that RNASE2, CX3CR1, and EPHX2 were independent prognostic variables for SP clinical outcomes. Through PPI network analysis, we assessed the interactions between these three independent prognostic variables (**Supplementary Fig. 1A**). The results of GO enrichment showed RNASE2, CX3CR1, and EPHX2 may be associated with biological functions such as chemotaxis and neuronal cell body membrane. KEGG enrichment analysis revealed that RNASE2, CX3CR1, and EPHX2 might be involved in the regulation of signaling

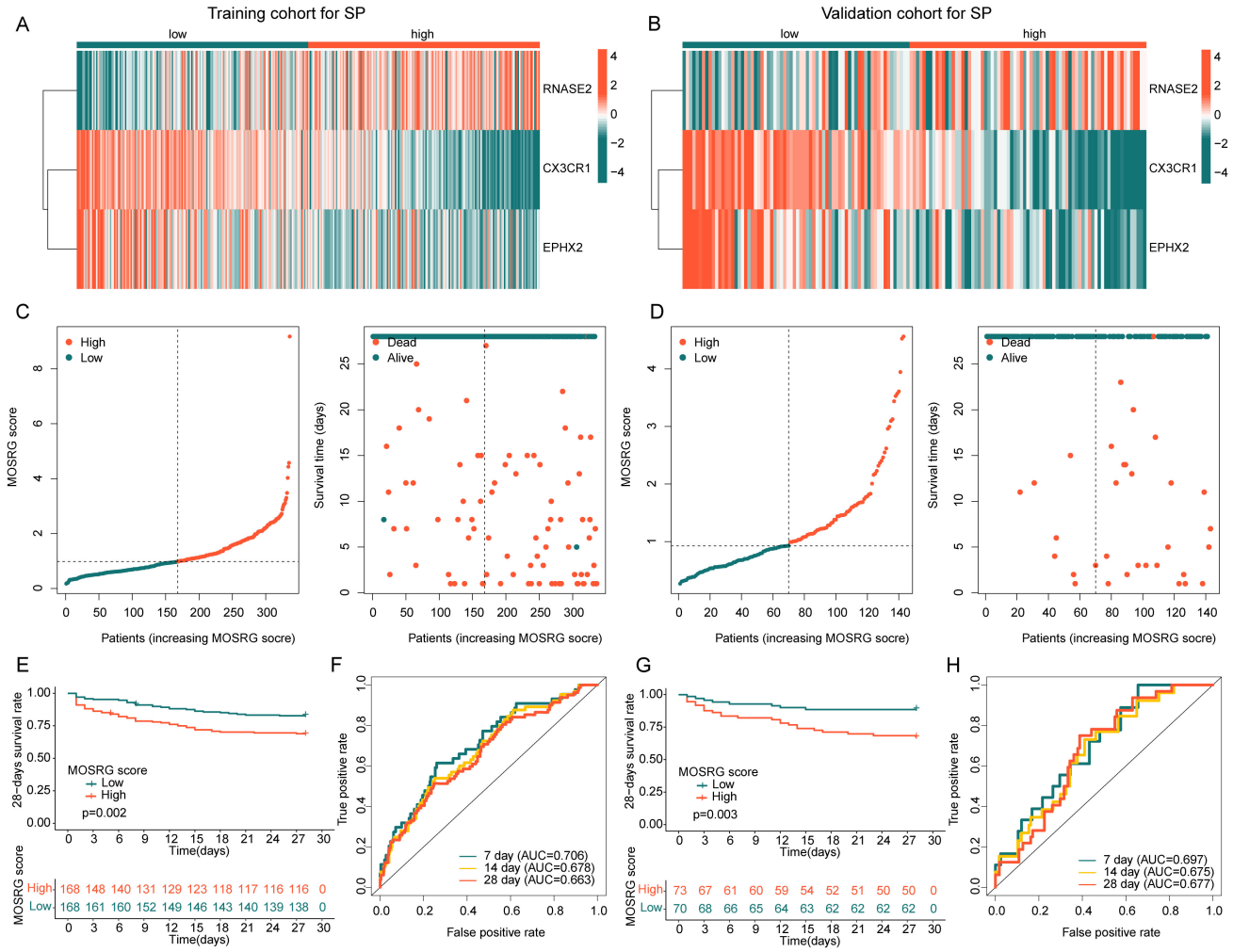

Fig. 4. Independence and stability validation of the MOSRG prognostic scoring model. (A,B) Expression analysis of MOSRG prognostic signatures. (C,D) Construction of the MOSRG prognostic scoring model in the training and validation cohorts. (E,F) Analysis of 28-day clinical survival curves and time-dependent ROC curves for sepsis samples in the training cohort. (G,H) Analysis of 28-day clinical survival curves and time-dependent ROC curves for sepsis samples in the validation cohort.

pathways such as arachidonic acid metabolism, peroxisome, and chemokine signaling pathway (**Supplementary Fig. 1B,C**). By conducting the risk coefficients and expression profiles of RNASE2, CX3CR1, and EPHX2, we developed a MOSRG scoring model for risk stratification in SP and to indicate clinical survival outcomes for different subgroups (Fig. 3C,D). PCA pattern analysis showed a distinct separation in the distribution patterns between MOSRG score subgroups, highlighting significant differences between them (Fig. 3E). Clinical survival curve analysis demonstrated that the 28-day survival rate in the low MOSRG subgroup was significantly higher, suggesting that SP samples in the low MOSRG subgroup may have better clinical survival benefits (Fig. 3F). Time-dependent ROC curve analysis showed area under the curve (AUC) values of 0.703, 0.677, and 0.666 for 7, 14, and 28 days, respectively, indicating a high diagnostic predictive ability (Fig. 3G).

3.4 Validation of the MOSRG Scoring System for Predicting Clinical Outcomes in Sepsis

Using the "caret" algorithm, we divided the 479 SP samples into training set and validation set at a 7:3 ratio and constructed the MOSRG scoring model to confirm the robustness and predictive performance of the MOSRG scoring system for clinical outcomes in sepsis patients. Based on *RNASE2*, *CX3CR1* and *EPHX2* risk coefficients and expression profiles, we developed the MOSRG scoring model in both cohorts and classified SP samples into two MOSRG scoring subgroups (Fig. 4A–D). In the training set, we observed that the 28-day clinical survival outcomes for the low MOSRG scoring subgroup were significantly better than those for the high MOSRG scoring subgroup (p = 0.002, Fig. 4E). Time-dependent ROC curve analysis indicated AUC values of 0.706, 0.678, and 0.663 for 7, 14, and 28 days, respectively (Fig. 4F). Notably, in the validation set, the 28-day survival outcomes for the low MOSRG scor-

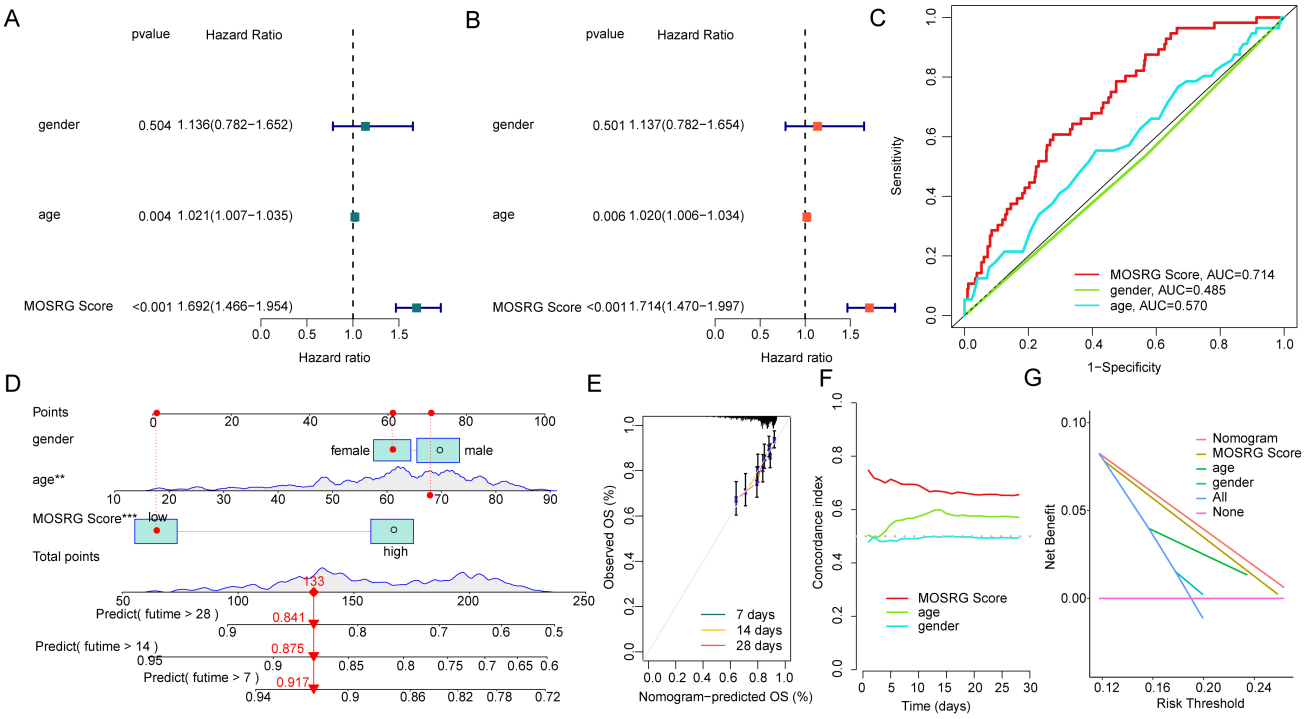

Fig. 5. Independent prognostic analysis and nomogram diagnostic model construction of the MOSRG scoring system. (A,B) Independent prognostic value assessment based on clinical-pathological features and MOSRG scoring. (C) ROC curve analysis for different variables. (D) Nomogram model construction. (E,F) Calibration curves and concordance index (C-index) evaluation. (G) The decision curve analysis (DCA) of different variables. $^{**}p < 0.01$, $^{***}p < 0.001$.

ing subgroup were also significantly superior to those for the high MOSRG scoring subgroup (p = 0.003, Fig. 4G). Time-dependent ROC curve analysis showed AUC values of 0.697, 0.675, and 0.677 for 7, 14, and 28 days, respectively (Fig. 4H). According to the survival analyses of both independent cohorts, we conclude that the MOSRG scoring system, constructed using MOSRG prognostic signatures, is capable of reliably predicting the 28-day survival outcomes.

3.5 MOSRG Scoring System Independent Prognostic Value Evaluation and Nomogram Model Development

By integrating the clinical and pathological characteristics of SP samples with the MOSRG scoring system, we evaluated the independent prognostic value. Univariate and multivariate cox regression indicated age and MOSRG score were associated with poor prognosis of SP (Fig. 5A,B). ROC curve analysis demonstrated that the AUC for the MOSRG score (0.714) was significantly higher than that for gender (AUC = 0.485) and age (AUC = 0.570), highlighting the superior prognostic capability of the MOSRG scoring system (Fig. 5C). Integrating the clinical and pathological characteristics with the MOSRG score, we constructed a nomogram to predict 7-, 14-, and 28-day survival probabilities (Fig. 5D). Calibration analysis revealed that the survival probabilities estimated by the nomogram were well-aligned with the actual survival rates of SP samples (Fig. 5E). The C-index curve results showed the accuracy of using the MOSRG scoring system to assess SP sample outcomes was significantly superior to that of age and gender (Fig. 5F). Moreover, the DCA analysis indicated that the nomogram model exhibited significantly higher accuracy in predicting clinical survival outcomes of SP compared to the MOSRG score and clinicopathological variables (Fig. 5G).

3.6 Immune Microenvironment Landscape in Different MOSRG Score Groups

Using the GSVA algorithm, we assessed potential mechanisms underlying survival outcome differences. The GSVA revealed that subgroup with low MOSRG score, pathways such as O-glycan biosynthesis and terpenoid backbone biosynthesis were significantly downregulated. A significant downregulation of multiple immune function-associated pathways, including the intestinal IgA immune network, T cell receptor (TCR) signaling, and NK cell-mediated cytotoxicity, was observed in the high MOSRG score subgroup (Fig. 6A). ESTIMATE showed subgroup with the high MOSRG score, immune scores and ESTIMATE scores were significantly lower, suggesting that SP samples in the high MOSRG score subgroup may exhibit a pronounced immunosuppressive state (Fig. 6B). Pearson's correlation analysis assessed potential links between MOSRG scores and immune microenvironment charac-

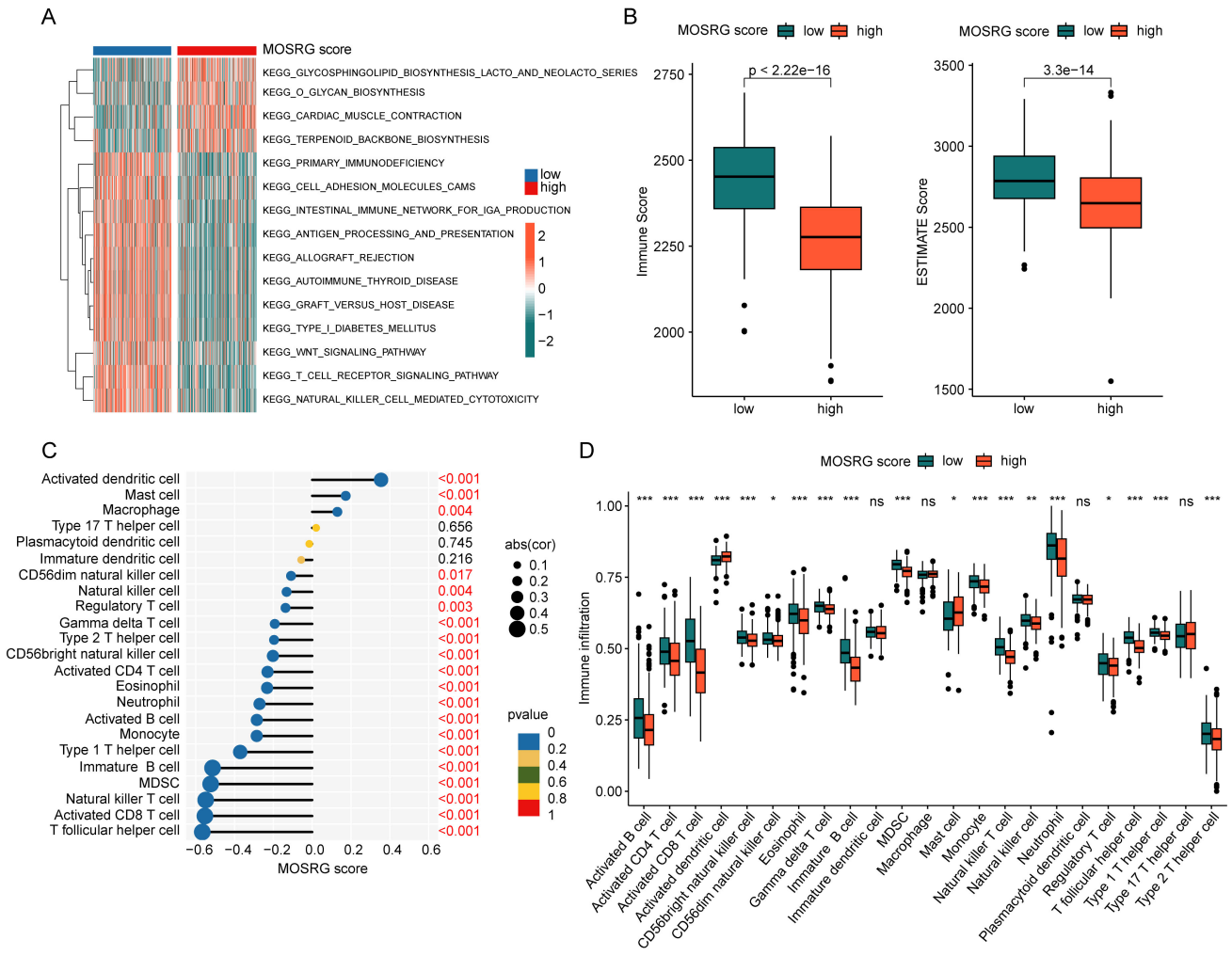

Fig. 6. Immune microenvironment landscape analysis of MOSRG scoring subgroups. (A) GSVA between MOSRG scoring subgroups. (B) Assessment of immune scores and ESTIMATE scores. (C) Correlation analysis between MOSRG scoring and immune microenvironment features. (D) Quantitative analysis of 23 types of immune infiltrating cells within MOSRG scoring subgroups. GSVA, Gene Set Variation Analysis; ESTIMATE, Estimation of STromal and Immune cells in MAlignant Tumor tissues using Expression data. *$p < 0.05$; **$p < 0.01$; ***$p < 0.001$; ns, not significant.

teristics, revealing a significant positive correlation with macrophages, mast cells, and activated dendritic cells, while showing a marked negative correlation with other immune infiltrating cells such as T follicular helper cells, activated $CD8^+$ T cells, natural killer T cells, myeloid-derived suppressor cells (MDSCs), and immature B cells (Fig. 6C). The quantitative assessment of immune cell infiltration showed that in the high MOSRG score subgroup, the infiltration levels of several immune cell types, such as activated B cells, $CD4^+$ T cells, $CD8^+$ T cells, and neutrophils, were significantly lower (Fig. 6D). Building on these results, we explored the possible interplay between the MOSRG score and immune microenvironmental features in sepsis, suggesting that reduced immune suppression may be linked to worse outcomes in sepsis.

3.7 Characterization of MOSRG Molecular Subtypes and Assessment of the Immune Microenvironment in Sepsis

We further identified the molecular subtyping landscape of MOSRG based on three MOSRGs prognostic variables (RNASE2, CX3CR1, and EPHX2). Using the optimal model parameters from consensus clustering analysis, we classified the sepsis samples into two distinct MOSRG molecular subgroups (k = 2). A total of 303 samples were assigned to Subgroup A, and 176 samples to Subgroup B (Fig. 7A–C). PCA revealed two clear separation patterns between the MOSRG molecular subgroups (Fig. 7D). The 28-day clinical survival curves indicated that samples in MOSRG Subgroup A had a longer overall survival time compared to those in Subgroup B (Fig. 7E). Additionally, we observed a significant increase in MOSRG scores in the poorer prognostic MOSRG subgroup, highlighting the possible interplay between the MOSRG scoring system and

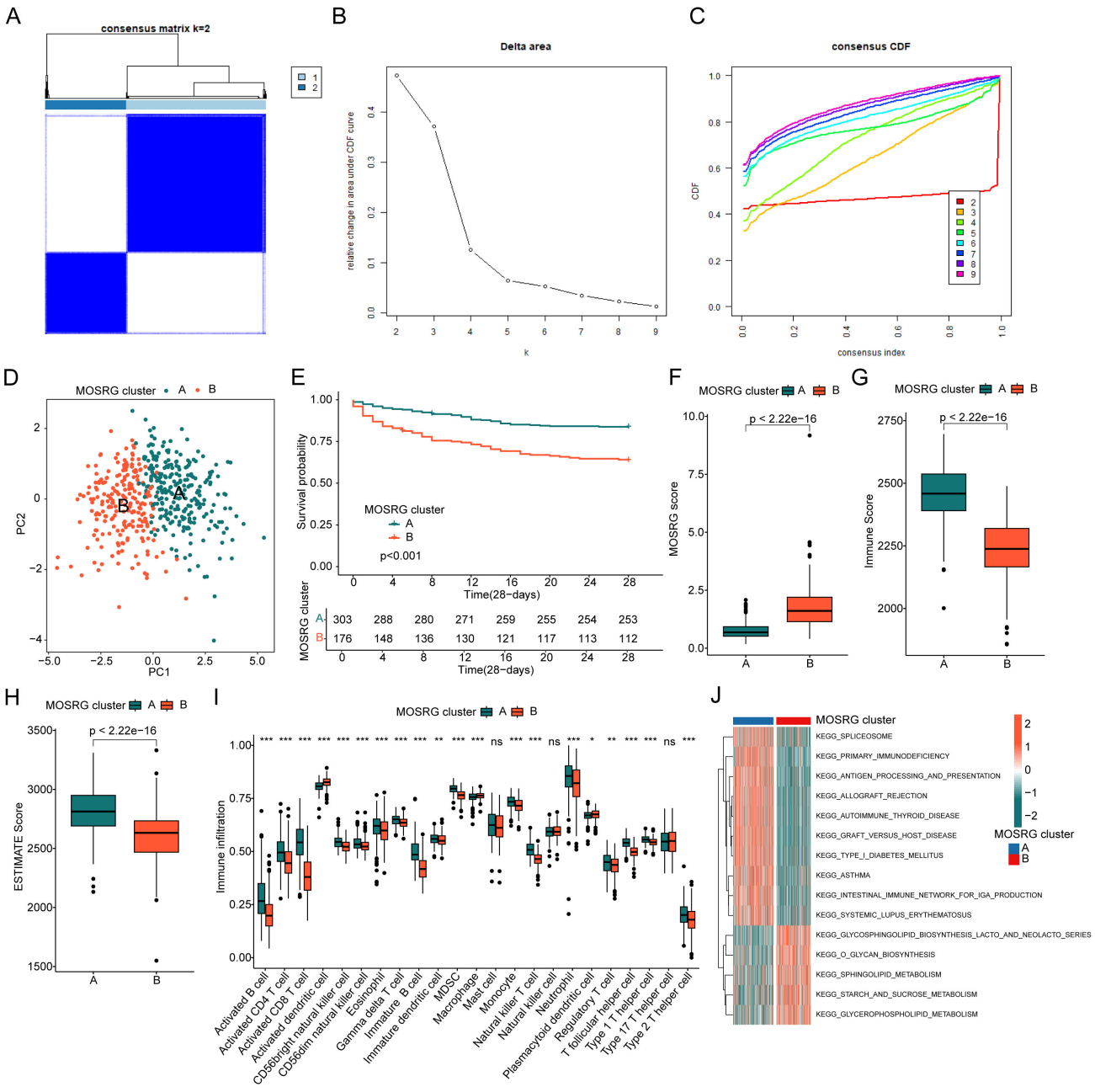

Fig. 7. Identification and profiling of MOSRG molecular subtypes and immune landscape in sepsis. (A–C) Identification of molecular subtype characteristics based on prognostic MOSRG signatures. (D) PCA pattern plot analysis. (E) Clinical prognosis curves for 28-day survival among MOSRG molecular subtypes. (F) Comparison of MOSRG Scores Across Different MOSRG Molecular Subtypes. (G,H) Assessment of immune scores and ESTIMATE scores within MOSRG molecular subtypes. (I) Quantitative analysis of the proportion of 23 types of immune cell infiltration. (J) GSVA elucidating differential regulation of KEGG signaling pathways between MOSRG molecular subtypes. CDF, cumulative distribution function. *$p < 0.05$; **$p < 0.01$; ***$p < 0.001$; ns, not significant.

molecular subgroups (Fig. 7F). Using ESTIMATE and ssGSEA immune infiltration algorithms, we explored potential distinctions in immune cell infiltration patterns between MOSRG molecular subgroups. Moreover, significantly higher immune scores and ESTIMATE scores could be observed in the subgroup with better prognosis, suggesting a pronounced immune activation state in this subgroup (Fig. 7G,H). Quantitative results indicated a significant increase in the proportion of various immune cells in MOSRG subgroup A (Fig. 7I). GSVA further revealed potential regulatory KEGG signaling pathways between MOSRG molecular subgroups. In the poorer prognostic MOSRG Subgroup B, immune regulation-related pathways were significantly downregulated, whereas metabolic pathways such as sucrose, starch, sphingolipid and glycerophospholipid metabolism were notably upregulated (Fig. 7J). Based on

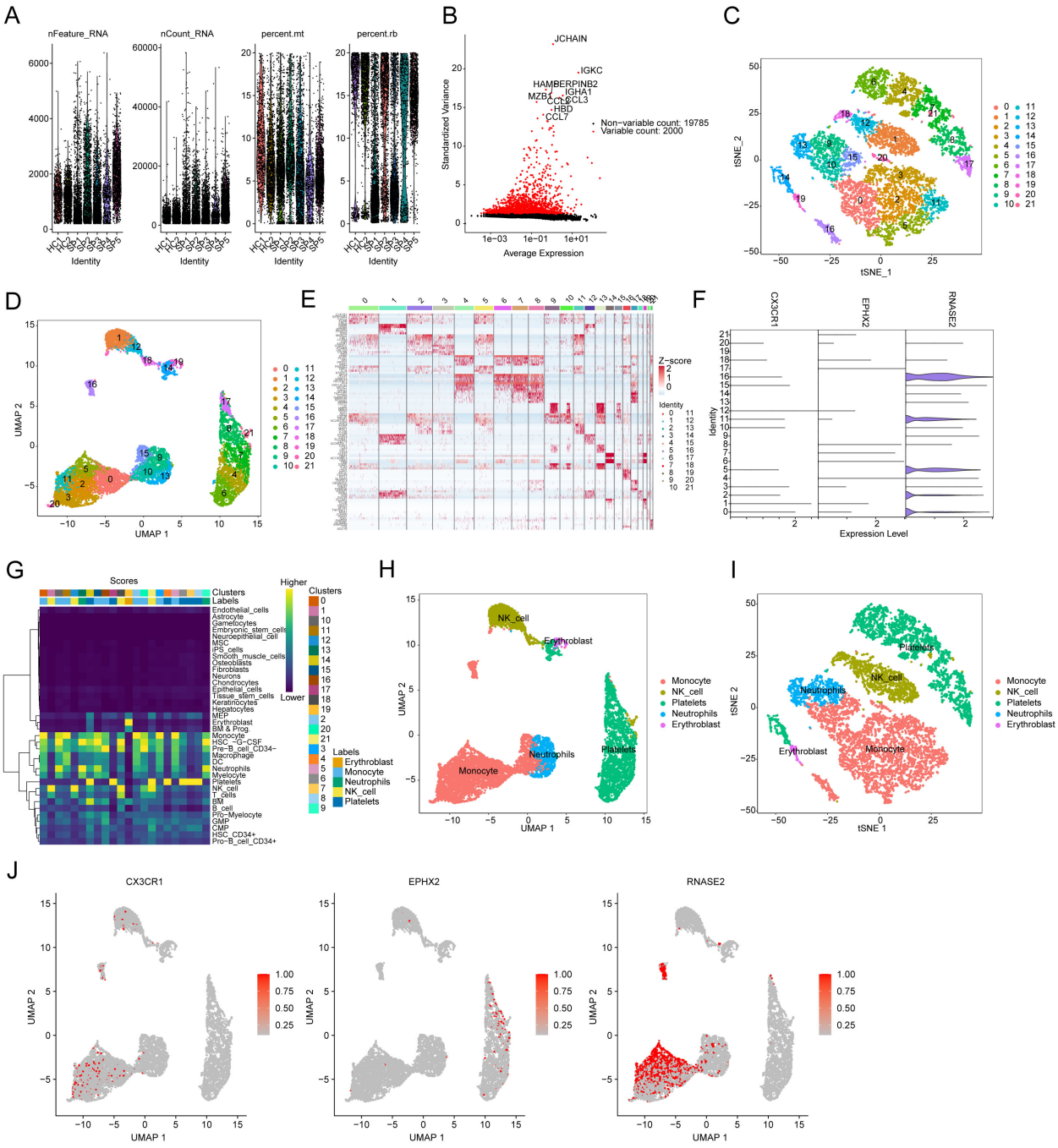

Fig. 8. Single-cell sequencing analysis of MOSRG prognostic signatures. (A) Quality control and normalization from HC (n = 2) and SP (n = 5) samples. (B) Variable genes identification. (C,D) tSNE and UMAP plots illustrating the distribution of 21 cell subtypes. (E) Expression analysis of marker genes for the 21 cell subtypes. (F) Expression of MOSRG prognostic signatures across the 21 cell subtypes. (G) Single-cell subtype annotation. (H,I) tSNE and UMAP plots depicting the distribution characteristics of 5 cell types. (J) Expression distribution of CX3CR1, EPHX2, and RNASE2 across the 5 cell types.

these results, we found that MOSRG-based prognostic signatures can accurately assess the MOSRG molecular subtype landscape in sepsis and indicate the clinical prognosis outcomes and immune microenvironment infiltration of different molecular subgroups.

3.8 Analysis of Single-Cell Sequencing Highlights the MOSRG Signatures in Distinct Cellular Subpopulations in Sepsis

We further analyzed the MOSRG prognostic signature characteristics within different cellular subpopulations of sepsis using single-cell sequencing analysis. By dataset GSE167363, we obtained scRNA-seq data from two HC

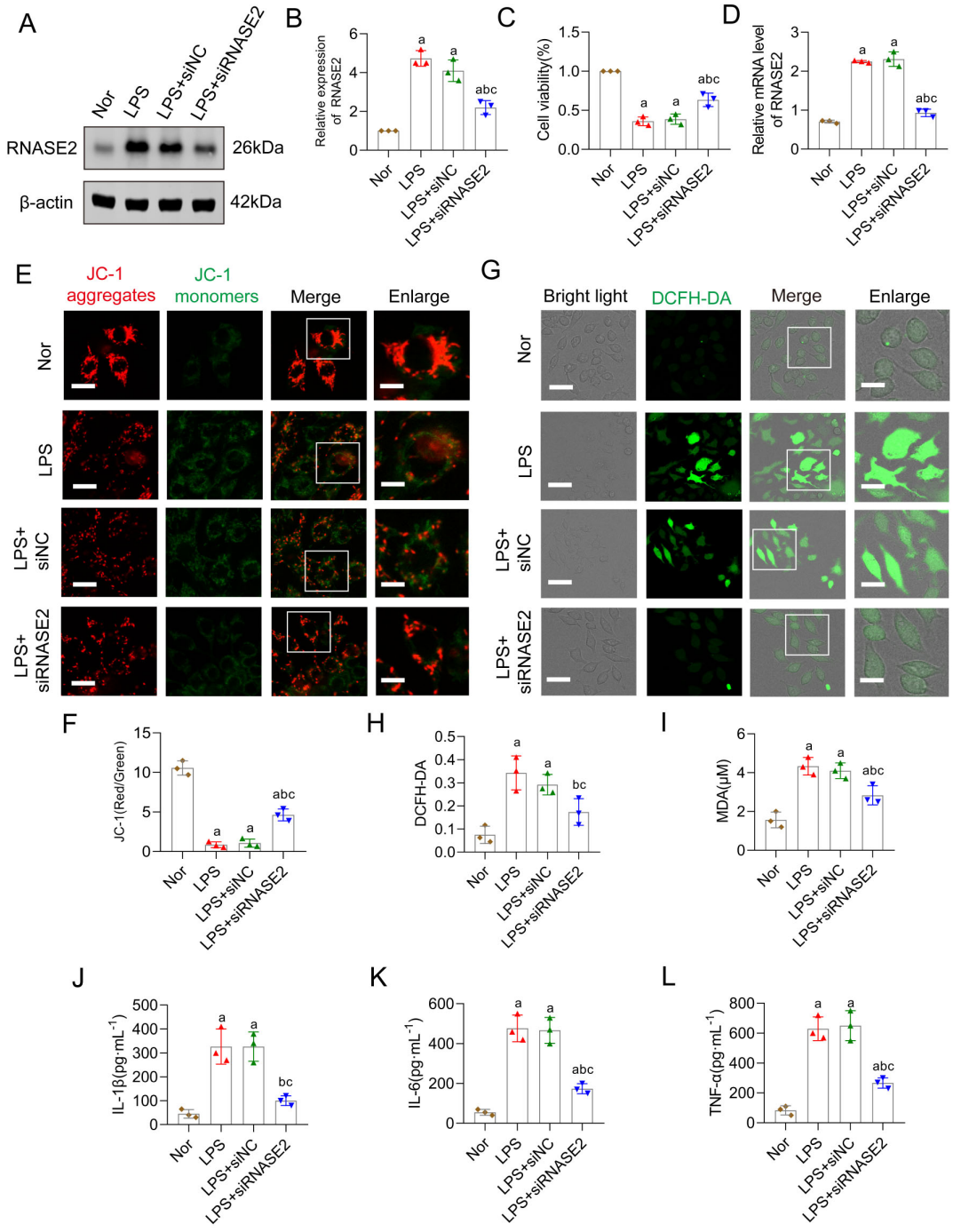

Fig. 9. RNASE2 inhibition attenuates mitochondrial oxidative stress of sepsis. (A,B) Western blots of RNASE2 in RAW264.7 macrophages following treatment with LPS (n = 3). (C) CCK-8 assay of RAW264.7 macrophages (n = 3). (D) Verification of interference efficiency of RNASE2 in RAW264.7 macrophages following treatment with LPS and siRNASE2 groups. (E,F) Mitochondrial membrane potential test by JC-1 aggregates and monomers, scale bars correspond to 20 μm for low-magnification images and 10 μm for high-magnification views (n = 3). (G,H) ROS immunofluorescent staining revealed oxidative stress levels in the cells, scale bars correspond to 40 μm for low-magnification images and 20 μm for high-magnification views (n = 3). (I) The MDA concentration in RAW264.7 macrophages was measured (n = 3). (J–L) Quantitative analysis of IL-1β, IL-6, and TNF-α in RAW264.7 macrophages (n = 3). a: $p <$ 0.05 as compared with the Normal group, b: $p < 0.05$ as compared with the LPS group, c: $p < 0.05$ as compared with the LPS+siNC group. LPS, lipopolysaccharide; siNC, negative control siRNA; CCK-8, Cell Counting Kit-8; JC-1, 5,5′,6,6′-Tetrachloro-1,1′,3,3′-tetraethylbenzimidazolylcarbocyanine iodide; ROS, reactive oxygen species; MDA, malondialdehyde; IL-1β, interleukin-1 beta; IL-6, interleukin-6; TNF-α, tumor necrosis factor-alpha.

and five SP. After quality control, we retained a sum of 38,562 high-quality cells for further analysis (Fig. 8A). Following normalization, we identified 2000 genes with high variability for dimensionality reduction analysis, including *JCHAIN*, *IGKC*, *HAMP*, *SERPINB2*, and *IGHA1* (Fig. 8B). Using the "FindAllMarkers" function, we identified marker genes for each cell subpopulation and visualized the distribution of 21 cell subpopulations using UMAP/tSNE dimensionality reduction plots (Fig. 8C–E). The violin plot results indicated that RNASE2, CX3CR1, and EPHX2 were expressed in all 21 cell subpopulations, with RNASE2 showing the most prominent expression (Fig. 8F). Cell annotation using SingleR revealed five cell subtypes in sepsis: monocytes, nature killer cells, platelets, neutrophils, and erythroblasts (Fig. 8G). The distribution features of these five cell subpopulations were further illustrated by UMAP and tSNE dimensionality reduction plots (Fig. 8H,I). We then analyzed the expression profile of MOSRG prognostic signatures within each cell subpopulation. UMAP results showed that CX3CR1 was observed in monocytes and NK cells, while EPHX2 was expressed in platelets. Notably, RNASE2 exhibited the most significant expression in monocytes (Fig. 8J).

3.9 Inhibiting RNASE2 can Effectively Improve Mitochondrial Oxidative Stress Damage in Sepsis

To examine the impact of RNASE2 on mitochondrial oxidative stress, we cultured macrophage cells and treated them with LPS to establish a sepsis model, utilizing siRNA to knock down RNASE2 expression. Western blotting (WB) results showed that compared to the Normal group, LPS stimulation upregulated RNASE2 levels, while siRNA effectively interfered with RNASE2 expression (Fig. 9A,B). LPS exposure significantly suppressed RAW264.7 macrophage viability, as determined by the CCK-8 assay, whereas interfering with RNASE2 effectively improved cell viability (Fig. 9C). In addition, we further verified the efficiency of the cell model interference at the mRNA level, and the PCR results suggested that the expression of RNASE2 in RAW264.7 macrophage was significantly reduced after RNASE interference compared with the LPS group (Fig. 9D). MDA, mitochondrial membrane potential, and ROS levels reflect cellular oxidative stress. Results indicated that oxidative stress levels in cell mitochondria significantly increased after LPS stimulation, manifested by elevated MDA levels, decreased mitochondrial membrane potential, and increased ROS production. However, interfering with RNASE2 effectively inhibited mitochondrial oxidative stress, reducing MDA and ROS levels and increasing mitochondrial membrane potential (Fig. 9E–I). Furthermore, we further investigated the changes in inflammatory mediators in RAW264.7 macrophages after RNASE2 interference. Compared to the model group, our result showed lower levels of IL-1β, IL-6, and TNF-α in RAW264.7 macrophages following siRNASE2 interference (Fig. 9J–L). Taken together, our findings suggest that inhibiting RNASE2 expression can significantly ameliorate mitochondrial oxidative stress damage in sepsis and reduce the occurrence of inflammation, highlighting the potential role of RNASE2 in sepsis.

4. Discussion

Sepsis is a life-threatening organ dysfunction with mortality rates reaching as high as 70% within three days of onset, which is related to a dysregulation of the immune response to pathogens [16]. Sustained hyperinflammation and immune suppression are key features of the pathophysiology of sepsis [17]. Despite the increasing understanding of the pathogenesis, clinical management of sepsis remains challenging due to antimicrobial resistance [18]. Further elucidation of the key molecular mechanisms is of great importance for finding potential clinical targets and therapeutic approaches to improve the overall prognosis of septic patients. In the present research, approximately 305 MOSRG were obtained, of which 59 MOSRG differed markedly between healthy and septic patients. Immediately afterwards, based on the DE-MOSRG, a risk prognosis model and MOSRG scoring model were constructed and validated for their excellent diagnostic value and ability to predict clinical outcomes in sepsis. Furthermore, we revealed a novel connection between MOSRG scoring model and abnormal immune infiltration in sepsis, suggesting that a lower level of immunosuppression might correlate with a poor prognosis for sepsis. The single-cell RNA sequencing results and *in vitro* experiments further indicated the great impact of *RNASE2* on the development of mitochondrial oxidative stress during sepsis. Our study identified potential biomarkers for sepsis diagnosis, offering crucial insights for sepsis diagnosis and treatment.

Previous study has demonstrated that mitochondrial dysfunction and heightened oxidative stress contribute to the progression of sepsis [19]. Clinical study has demonstrated a great correlation between mitochondrial dysfunction and higher mortality in septic patients [20]. Profound metabolic disturbances of the redox system were observed in sepsis, leading to mitochondria oxidative stress. Acute inflammatory responses in sepsis may cause oxidative stress, contributing to microcirculatory dysfunction, tissue damage, acute respiratory failure, multi-organ failure, which may result in death [21,22]. In this work, we mainly focused on MOSRG in sepsis. Three MOSRGs (*RNASE2*, *CX3CR1* and *EPHX2*) were recognized as independent prognostic indicators for sepsis through univariate and multivariate Cox regression, as well as LASSO regression. We also established MOSRG scoring model based on three MOSRGs to accurately assess survival characteristics, which could improve clinical outcome predictions in sepsis. As an RNA-binding protein, ribonuclease 2 (*RNASE2*) belongs to the *RNase A* superfamily [23]. It was secreted by eosinophilic cytoplasmic granules, most

abundant in macrophages and leukocytes [24]. Studies have documented that *RNASE2* participated in human inflammatory responses, which showed immune-modulating properties against multiple pathogens [25,26]. It also proposed that *RNASE2* participated in the host response against the single-stranded RNA virus, such as adenoviruses, retroviruses and rhinoviruses, even HIV [27]. As a G-protein-coupled receptor, CX3C chemokine receptor 1 (*CX3CR1*) is expressed by $CD8^+$ T lymphocytes, natural killer cells, microglial cells, neurons, mast cells and monocytes [28]. A previous study indicated the potential involvement of *CX3CR1* in inflammatory disorders such as atherosclerosis and arthritis by mediating inflammation [29]. Reduced CX3CR1 expression has been identified as an independent molecular biomarker associated with both early and late mortality in critically ill patients [30]. The expression of *CX3CR1* was downregulated on circulating monocytes in septic shock patients, suggesting that *CX3CR1* may constitute a novel characteristic of sepsis-induced immunosuppression [31]. Soluble epoxide hydrolase 2 (*EPHX2*) is encoded by *EPHX2* gene, which is widely distributed in tissues, particularly kidney and liver. EPHX2 has been proposed as a potential susceptibility gene for atherosclerosis and is increasingly recognized as a promising therapeutic target in various immune-metabolic disorders [32,33]. Reduced EPHX2 expression is associated with the extent of inflammation during disease progression. EPHX2 metabolizes anti-inflammatory epoxyeicosatrienoic acids (EETs) into their less active dihydroxyeicosatrienoic acid (DHET) forms, thereby promoting pro-inflammatory effects [34]. Collectively, these studies indicate that dysregulated expression of the three MOSRGs is strongly associated with inflammation and related pathological conditions, suggesting their potential diagnostic significance in sepsis.

Immunosuppression and the excessive inflammatory response caused by reactivation of primary infections have been identified by epidemiological study as principal drivers of mortality in septic patients [35]. Previous reports have suggested that modulation of oxidative stress can effectively regulate inflammatory responses and enhance survival outcomes in sepsis [13,36]. We found that the immune functions-related signaling pathways were considerably downregulated in the high-MOSRG score subgroup. Simultaneously, our data showed a remarkable state of immunosuppression with decreased infiltrated immune cells in high-MOSRG score sepsis sample. Collectively, our findings provide additional evidence that a lower immunosuppressive state is associated with poorer prognosis in septic patients.

Mitochondrial dysfunction is not only a hallmark of sepsis-related organ damage but also serves as a key regulator of neuroinflammation and cognitive impairment [37]. In sepsis, excessive mitochondrial ROS production triggers an oxidative stress storm, leading to widespread cellular damage and disruption of the blood-brain barrier (BBB) [38]. The disruption of the BBB is a critical pathological event linking systemic inflammation to central nervous system dysfunction in sepsis. Sepsis-induced BBB breakdown is mediated by multiple mechanisms, including oxidative stress-induced endothelial damage, increased pro-inflammatory cytokine production, and matrix metalloproteinase (MMP) activation, leading to tight junction degradation [39]. Disruption of the BBB permits the infiltration of peripheral inflammatory mediators and immune cells into the central nervous system, thereby aggravating neuroinflammation [40]. Persistent oxidative stress and mitochondrial dysfunction within the brain promote neuronal apoptosis, synaptic dysfunction, and impairments in neuroplasticity, ultimately contributing to long-term cognitive decline [41,42]. Therefore, mitochondrial oxidative stress acts as a critical upstream event linking systemic inflammation to central nervous system damage during sepsis development. Notably, the findings of this study may also have important implications for neonatal patients. Neonates are particularly vulnerable to mitochondrial dysfunction and oxidative stress due to the immaturity of their antioxidant defense systems [43,44]. Mitochondrial dysregulation and excessive oxidative stress contribute significantly to neurodevelopmental impairments in neonatal sepsis survivors [45,46]. It is conceivable that targeting mitochondrial pathways could offer novel therapeutic strategies for mitigating long-term cognitive and developmental deficits in neonates affected by sepsis.

Single-cell RNA sequencing technology offers excellent opportunities for identifying biomarkers and signaling pathways in infectious diseases, thereby facilitating the elucidation of molecular mechanisms underlying immune regulation [47]. By using single-cell RNA-seq, we identified three MOSRGs as significantly differentially expressed in the 21 immune cell subpopulations, while *RNASE2* exhibited the remarkable elevation, particularly in monocytes. It is well known that *RNASE2* is a key contributor to host defense against pathogens and is particularly abundant in the human acute monocytic leukemia cell line (THP-1) among the blood cell types [48]. RNASE2 has a central function in the host immune response, exerting both direct antimicrobial effects against a broad spectrum of pathogens and various immunomodulatory functions [7]. Yang and colleagues have characterized that *RNASE2* was a chemoattractant for $CD34^+$ progenitor-derived dendritic cells [49]. As an alarmin, RNASE2 is an endogenous molecule that interacts with pattern recognition receptors, triggering signals of tissue and cell damage [50]. Our *in vitro* results showed the expression of *RNASE2* was significantly elevated with markedly elevated mitochondrial oxidative stress level after the LPS stimulation, whilst interfering with the expression of *RNASE2* could effectively reverse the observed effects. Based on the findings above, further investigation into the role of RNASE2 in sepsis diagnosis would be highly valuable.

In conclusion, we identified three MOSRGs as potential diagnostic biomarkers for sepsis. Immune infiltration analysis provided strong evidence that these biomarkers are closely associated with immune-related mechanisms underlying sepsis pathogenesis. Among them, RNASE2 emerged as a key regulator of mitochondrial oxidative stress, as demonstrated by single-cell RNA sequencing and *in vitro* molecular experiments. Specifically, RNASE2 was shown to modulate ROS and MDA levels under septic conditions. However, due to the lack of patient-level correlation data, the clinical relevance of RNASE2 in human sepsis remains speculative. Additionally, despite the multi-step feature selection process, the limited sample size relative to the number of input variables may still pose a risk of overfitting, and external validation is needed to confirm the robustness of the prognostic model. Another limitation of our study is that some continuous variables, such as age and nomogram scores, were binarized before being included in the prediction model. This binarization, while simplifying the model, led to predicted probabilities with only two possible values (0 or 1), which in turn resulted in DCA plots that appear as piecewise linear or straight lines. Although this approach may facilitate interpretation in clinical settings, it can potentially reduce the granularity and accuracy of the model's predictive output. Future studies may benefit from incorporating continuous variables directly or exploring alternative modeling strategies to preserve predictive information and enhance the interpretability of DCA results. Overall, our findings shed light on the molecular landscape of MOSRG in sepsis and propose novel targets for its diagnosis and therapeutic intervention.

5. Conclusion

In conclusion, this study systematically elucidates the critical role of mitochondrial oxidative stress-related genes in the pathogenesis and immune regulation of sepsis through integrative bioinformatics analysis and experimental validation. RNASE2 was demonstrated to aggravate mitochondrial oxidative stress in sepsis, and its inhibition alleviated oxidative injury, suggesting a promising therapeutic target. These findings provide new insights into the molecular mechanisms underlying sepsis and offer a foundation for the development of novel diagnostic and therapeutic strategies.

Availability of Data and Materials

All data generated or analyzed during this study are included in this published article and its supplementary information files.

Author Contributions

YW and BZ created the study concept and design. BZ contributed to data collection, experimental design, and data analysis. JW conceived the original ideas and composed this manuscript. YW contributed to the table and figures in this manuscript. All authors contributed to editorial changes in the manuscript. All authors read and approved the final manuscript. All authors have participated sufficiently in the work and agreed to be accountable for all aspects of the work.

Ethics Approval and Consent to Participate

GEO database belongs to public databases. Users can download relevant data for free for research and publish relevant articles. Our study is based on open-source data, so there are no ethical issues and other conflicts of interest.

Acknowledgment

Not applicable.

Funding

This research received no external funding.

Conflict of Interest

The authors declare no conflict of interest.

Supplementary Material

Supplementary material associated with this article can be found, in the online version, at https://doi.org/10.31083/FBL38957.

References

[1] Brizuela V, Cuesta C, Bartolelli G, Abdosh AA, Abou Malham S, Assarag B, *et al*. Availability of facility resources and services and infection-related maternal outcomes in the WHO Global Maternal Sepsis Study: a cross-sectional study. The Lancet. Global Health. 2021; 9: e1252–e1261. https://doi.org/10.1016/S2214-109X(21)00248-5.

[2] Cecconi M, Evans L, Levy M, Rhodes A. Sepsis and septic shock. Lancet (London, England). 2018; 392: 75–87. https://doi.org/10.1016/S0140-6736(18)30696-2.

[3] Prescott HC, Angus DC. Enhancing Recovery From Sepsis: A Review. JAMA. 2018; 319: 62–75. https://doi.org/10.1001/jama.2017.17687.

[4] Dugar S, Choudhary C, Duggal A. Sepsis and septic shock: Guideline-based management. Cleveland Clinic Journal of Medicine. 2020; 87: 53–64. https://doi.org/10.3949/ccjm.87a.18143.

[5] van der Poll T, Shankar-Hari M, Wiersinga WJ. The immunology of sepsis. Immunity. 2021; 54: 2450–2464. https://doi.org/10.1016/j.immuni.2021.10.012.

[6] Singer M. The role of mitochondrial dysfunction in sepsis-induced multi-organ failure. Virulence. 2014; 5: 66–72. https://doi.org/10.4161/viru.26907.

[7] Arulkumaran N, Deutschman CS, Pinsky MR, Zuckerbraun B, Schumacker PT, Gomez H, *et al*. MITOCHONDRIAL FUNCTION IN SEPSIS. Shock (Augusta, Ga.). 2016; 45: 271–281. https://doi.org/10.1097/SHK.0000000000000463.

[8] West AP, Brodsky IE, Rahner C, Woo DK, Erdjument-Bromage H, Tempst P, *et al*. TLR signalling augments macrophage bactericidal activity through mitochondrial ROS. Nature. 2011; 472: 476–480. https://doi.org/10.1038/nature09973.

[9] Santos SS, Brunialti MKC, Rigato O, Machado FR, Silva E, Salomao R. Generation of nitric oxide and reactive oxygen species by neutrophils and monocytes from septic patients and association with outcomes. Shock (Augusta, Ga.). 2012; 38: 18–23. https://doi.org/10.1097/SHK.0b013e318257114e.

[10] Kong X, Thimmulappa R, Kombairaju P, Biswal S. NADPH oxidase-dependent reactive oxygen species mediate amplified TLR4 signaling and sepsis-induced mortality in Nrf2-deficient mice. Journal of Immunology (Baltimore, Md.: 1950). 2010; 185: 569–577. https://doi.org/10.4049/jimmunol.0902315.

[11] Chen XH, Yin YJ, Zhang JX. Sepsis and immune response. World Journal of Emergency Medicine. 2011; 2: 88–92.

[12] Shenoy S. Coronavirus (Covid-19) sepsis: revisiting mitochondrial dysfunction in pathogenesis, aging, inflammation, and mortality. Inflammation Research. 2020; 69: 1077–1085. https://doi.org/10.1007/s00011-020-01389-z.

[13] Bulua AC, Simon A, Maddipati R, Pelletier M, Park H, Kim KY, *et al*. Mitochondrial reactive oxygen species promote production of proinflammatory cytokines and are elevated in TNFR1-associated periodic syndrome (TRAPS). The Journal of Experimental Medicine. 2011; 208: 519–533. https://doi.org/10.1084/jem.20102049.

[14] Wu H, Tang T, Deng H, Chen D, Zhang C, Luo J, *et al*. Immune checkpoint molecule Tim-3 promotes NKT cell apoptosis and predicts poorer prognosis in Sepsis. Clinical Immunology (Orlando, Fla.). 2023; 254: 109249. https://doi.org/10.1016/j.clim.2023.109249.

[15] Qiu X, Li J, Bonenfant J, Jaroszewski L, Mittal A, Klein W, *et al*. Dynamic changes in human single-cell transcriptional signatures during fatal sepsis. Journal of Leukocyte Biology. 2021; 110: 1253–1268. https://doi.org/10.1002/JLB.5MA0721-825R.

[16] van der Poll T, van de Veerdonk FL, Scicluna BP, Netea MG. The immunopathology of sepsis and potential therapeutic targets. Nature Reviews. Immunology. 2017; 17: 407–420. https://doi.org/10.1038/nri.2017.36.

[17] Yao RQ, Ren C, Zheng LY, Xia ZF, Yao YM. Advances in Immune Monitoring Approaches for Sepsis-Induced Immunosuppression. Frontiers in Immunology. 2022; 13: 891024. https://doi.org/10.3389/fimmu.2022.891024.

[18] van der Poll T. Future of sepsis therapies. Critical Care (London, England). 2016; 20: 106. https://doi.org/10.1186/s13054-016-1274-9.

[19] Mayorov V, Uchakin P, Amarnath V, Panov AV, Bridges CC, Uzhachenko R, *et al*. Targeting of reactive isolevuglandins in mitochondrial dysfunction and inflammation. Redox Biology. 2019; 26: 101300. https://doi.org/10.1016/j.redox.2019.101300.

[20] Brealey D, Brand M, Hargreaves I, Heales S, Land J, Smolenski R, *et al*. Association between mitochondrial dysfunction and severity and outcome of septic shock. Lancet (London, England). 2002; 360: 219–223. https://doi.org/10.1016/S0140-6736(02)09459-X.

[21] Galley HF. Oxidative stress and mitochondrial dysfunction in sepsis. British Journal of Anaesthesia. 2011; 107: 57–64. https://doi.org/10.1093/bja/aer093.

[22] Nagar H, Piao S, Kim CS. Role of Mitochondrial Oxidative Stress in Sepsis. Acute and Critical Care. 2018; 33: 65–72. https://doi.org/10.4266/acc.2018.00157.

[23] Cho S, Beintema JJ, Zhang J. The ribonuclease A superfamily of mammals and birds: identifying new members and tracing evolutionary histories. Genomics. 2005; 85: 208–220. https://doi.org/10.1016/j.ygeno.2004.10.008.

[24] Barnard EA. Biological function of pancreatic ribonuclease. Nature. 1969; 221: 340–344. https://doi.org/10.1038/221340a0.

[25] Rosenberg HF. Eosinophil-Derived Neurotoxin (EDN/RNase 2) and the Mouse Eosinophil-Associated RNases (mEars): Expanding Roles in Promoting Host Defense. International Journal of Molecular Sciences. 2015; 16: 15442–15455. https://doi.org/10.3390/ijms160715442.

[26] Lu L, Li J, Moussaoui M, Boix E. Immune Modulation by Human Secreted RNases at the Extracellular Space. Frontiers in Immunology. 2018; 9: 1012. https://doi.org/10.3389/fimmu.2018.01012.

[27] Rosenberg HF, Domachowske JB. Eosinophils, ribonucleases and host defense: solving the puzzle. Immunologic Research. 1999; 20: 261–274. https://doi.org/10.1007/BF02790409.

[28] Kim KW, Vallon-Eberhard A, Zigmond E, Farache J, Shezen E, Shakhar G, *et al*. In vivo structure/function and expression analysis of the CX3C chemokine fractalkine. Blood. 2011; 118: e156–e167. https://doi.org/10.1182/blood-2011-04-348946.

[29] Yano R, Yamamura M, Sunahori K, Takasugi K, Yamana J, Kawashima M, *et al*. Recruitment of CD16+ monocytes into synovial tissues is mediated by fractalkine and CX3CR1 in rheumatoid arthritis patients. Acta Medica Okayama. 2007; 61: 89–98. https://doi.org/10.18926/AMO/32882.

[30] Friggeri A, Cazalis MA, Pachot A, Cour M, Argaud L, Allaouchiche B, *et al*. Decreased CX3CR1 messenger RNA expression is an independent molecular biomarker of early and late mortality in critically ill patients. Critical Care (London, England). 2016; 20: 204. https://doi.org/10.1186/s13054-016-1362-x.

[31] Pachot A, Cazalis MA, Venet F, Turrel F, Faudot C, Voirin N, *et al*. Decreased expression of the fractalkine receptor CX3CR1 on circulating monocytes as new feature of sepsis-induced immunosuppression. Journal of Immunology (Baltimore, Md.: 1950). 2008; 180: 6421–6429. https://doi.org/10.4049/jimmunol.180.9.6421.

[32] Wagner K, Yang J, Inceoglu B, Hammock BD. Soluble epoxide hydrolase inhibition is antinociceptive in a mouse model of diabetic neuropathy. The Journal of Pain. 2014; 15: 907–914. https://doi.org/10.1016/j.jpain.2014.05.008.

[33] Pillarisetti S, Khanna I. Targeting soluble epoxide hydrolase for inflammation and pain - an overview of pharmacology and the inhibitors. Inflammation & Allergy Drug Targets. 2012; 11: 143–158. https://doi.org/10.2174/187152812800392823.

[34] Das UN. Arachidonic acid in health and disease with focus on hypertension and diabetes mellitus: A review. Journal of Advanced Research. 2018; 11: 43–55. https://doi.org/10.1016/j.jare.2018.01.002.

[35] Delano MJ, Ward PA. Sepsis-induced immune dysfunction: can immune therapies reduce mortality? The Journal of Clinical Investigation. 2016; 126: 23–31. https://doi.org/10.1172/JCI82224.

[36] Liu D, Huang SY, Sun JH, Zhang HC, Cai QL, Gao C, *et al*. Sepsis-induced immunosuppression: mechanisms, diagnosis and current treatment options. Military Medical Research. 2022; 9: 56. https://doi.org/10.1186/s40779-022-00422-y.

[37] Zhang G, Wei H, Zhao A, Yan X, Zhang X, Gan J, *et al*. Mitochondrial DNA leakage: underlying mechanisms and therapeutic implications in neurological disorders. Journal of Neuroinflammation. 2025; 22: 34. https://doi.org/10.1186/s12974-025-03363-0.

[38] Kim S, Jung UJ, Kim SR. Role of Oxidative Stress in Blood-Brain Barrier Disruption and Neurodegenerative Diseases. Antioxidants (Basel, Switzerland). 2024; 13: 1462. https://doi.org/10.3390/antiox13121462.

[39] Nwafor DC, Brichacek AL, Mohammad AS, Griffith J, Lucke-Wold BP, Benkovic SA, *et al*. Targeting the Blood-Brain Barrier to Prevent Sepsis-Associated Cognitive Impairment. Journal of Central Nervous System Disease. 2019; 11: 1179573519840652. https://doi.org/10.1177/1179573519840652.

[40] Sun B, Li L, Harris OA, Luo J. Blood-brain barrier dis-

ruption: a pervasive driver and mechanistic link between traumatic brain injury and Alzheimer's disease. Translational Neurodegeneration. 2025; 14: 16. https://doi.org/10.1186/s40035-025-00478-5.

[41] Zhang Z, Yang W, Wang L, Zhu C, Cui S, Wang T, *et al*. Unraveling the role and mechanism of mitochondria in postoperative cognitive dysfunction: a narrative review. Journal of Neuroinflammation. 2024; 21: 293. https://doi.org/10.1186/s12974-024-03285-3.

[42] Joshi DC, Chavan MB, Gurow K, Gupta M, Dhaliwal JS, Ming LC. The role of mitochondrial dysfunction in Huntington's disease: Implications for therapeutic targeting. Biomedicine & Pharmacotherapy = Biomedecine & Pharmacotherapie. 2025; 183: 117827. https://doi.org/10.1016/j.biopha.2025.117827.

[43] You Q, Lan XB, Liu N, Du J, Ma L, Yang JM, *et al*. Neuroprotective strategies for neonatal hypoxic-ischemic brain damage: Current status and challenges. European Journal of Pharmacology. 2023; 957: 176003. https://doi.org/10.1016/j.ejphar.2023.176003.

[44] Perez M, Robbins ME, Revhaug C, Saugstad OD. Oxygen radical disease in the newborn, revisited: Oxidative stress and disease in the newborn period. Free Radical Biology & Medicine. 2019; 142: 61–72. https://doi.org/10.1016/j.freeradbiomed.2019.03.035.

[45] Chen J, Yasrebinia S, Ghaedi A, Khanzadeh M, Quintin S, Dagra A, *et al*. Meta-analysis of the role of neutrophil to lymphocyte ratio in neonatal sepsis. BMC Infectious Diseases. 2023; 23: 837. https://doi.org/10.1186/s12879-023-08800-0.

[46] Ildarabadi A, Mir Mohammad Ali SN, Rahmani F, Mosavari N, Pourbakhtyaran E, Rezaei N. Inflammation and oxidative stress in epileptic children: from molecular mechanisms to clinical application of ketogenic diet. Reviews in the Neurosciences. 2024; 35: 473–488. https://doi.org/10.1515/revneuro-2023-0128.

[47] Uyar O, Dominguez JM, Bordeleau M, Lapeyre L, Ibáñez FG, Vallières L, *et al*. Single-cell transcriptomics of the ventral posterolateral nucleus-enriched thalamic regions from HSV-1-infected mice reveal a novel microglia/microglia-like transcriptional response. Journal of Neuroinflammation. 2022; 19: 81. https://doi.org/10.1186/s12974-022-02437-7.

[48] Lu L, Li J, Wei R, Guidi I, Cozzuto L, Ponomarenko J, *et al*. Selective cleavage of ncRNA and antiviral activity by RNase2/EDN in THP1-induced macrophages. Cellular and Molecular Life Sciences: CMLS. 2022; 79: 209. https://doi.org/10.1007/s00018-022-04229-x.

[49] Yang D, Rosenberg HF, Chen Q, Dyer KD, Kurosaka K, Oppenheim JJ. Eosinophil-derived neurotoxin (EDN), an antimicrobial protein with chemotactic activities for dendritic cells. Blood. 2003; 102: 3396–3403. https://doi.org/10.1182/blood-2003-01-0151.

[50] Bianchi ME. DAMPs, PAMPs and alarmins: all we need to know about danger. Journal of Leukocyte Biology. 2007; 81: 1–5. https://doi.org/10.1189/jlb.0306164.